The Eurasia Proceedings of Science, Technology, Engineering & Mathematics (EPSTEM)
ISSN: 2602-3199

The Eurasia Proceedings of Science, Technology, Engineering & Mathematics (EPSTEM), 2024

Volume 32, Pages 173-184

IConTES 2024: International Conference on Technology, Engineering and Science

Numerical Damage Prediction of Marine Structures Reinforced by Composite Patch with XFEM and CZM Methods

Harmel Mohammed Walid
Djilali Liabes University of Sidi-Bel-Abbes

Zouggar Kamel
Djilali Liabes University of Sidi-Bel-Abbes

Baghdadi Mohammed
Djilali Liabes University of Sidi-Bel-Abbes

Mhamdia Rachid
Djilali Liabes University of Sidi-Bel-Abbes

Abstract: The present work presents the numerical model of a marine steel with a hole repaired by a bonded composite patch. For modelling, Extended Finite Element Method (XFEM) technique is used in conjunction with the Cohesive Zone Model (CZM) to perform the damage analyses of different adhesives used in the repair of marine steels. The main objective of the study is to analyse the mechanical behaviour of the repair and compare different types of composite adhesives in order to optimize this kind of repair design. Numerical modelling is used in order to assess the stresses, strains, initiation, and propagation of damage in the repaired assembly. The mechanical performance test of the specimen proved that the mechanical performance of the repair is strongly dependent on the choice of the composite adhesive. Some adhesives possess better mechanical strength and a high resistance to damage compared to other kinds of adhesives. These results will provide important data in guiding the selection of materials for designing composite patch repairs on marine steel structures.

Keywords: Marine steel, Composite patch repair, Cohesive zone model, Adhesive damage.

Introduction

In general, the degradation of structures in extreme environments is a major problem in a number of fields, such as the maritime, the aeronautical and the civil engineering sectors (Karatzas, 2016). This can cause cracks and significant damage throughout the life of the structures. Due to its excellent mechanical properties, which provide good resistance to the harsh operating conditions, the majority of marine structures are made of steel. In spite of these advantages, steel remains particularly susceptible to the cumulative effects of corrosion and fatigue, which are exacerbated by prolonged exposure to the marine environment and which accelerate the propagation of cracks and increase the risk of structural failure (Feng et al., 2020; Abbas & Shafiee, 2020).

Many recent experimental studies have been instrumental in improving the reliability of this method to increase the strength and durability of damaged structures (Silva et al., 2023; Liu et al., 2022; Karatzas, Kotsidis, & Tsouvalis, 2015; Mishra, Lal, & Sutaria, 2023). Research by Madani et al. (2010) shows that patch repair can reduce the stress concentration around notches in a reinforced plate, with a lower total amount of strain. Furthermore, the use of CFRP patches was found to effectively limit crack propagation and extend the fatigue life of steel structures by Yu et al. (2014). However, according to Benyahia et al. (2015) the performance of the

repair decreases with increasing soaking time. Li et al. (2019) found that the square shaped patch gave the best performance. Berrahou and Amari (2022) investigated different patch types and shapes for the repair of notched composite panels, identifying the boron/epoxy and solid configurations as the optimal options. (Riveros et al., 2022). Demonstrate that a basalt fiber patch (BFRP) significantly improves the service life of repaired structures.

Meanwhile, numerical simulations using FEM modelling software such as Abaqus and Ansys have been instrumental in the analysis and improvement of repair techniques (Kaddouri et al., 2020; Breitzman et al., 2009; Fekih et al., 2012; Iváñez & Braun, 2018; Zhang et al., 2018), investigated the stress distribution in the adhesive for different crack lengths. Their results effectively predicted failure in the adhesive. Moreover, the boron/epoxy circular patch was identified as the best solution for the repair of aluminium alloy marine structures by Sadek et al. (2018). In addition, Shivaie -Kojouri et al. (2023) carried out a comparative study between aged and non-aged composite patches, which highlighted the effect of ageing on the performance of the repair.

Advanced modelling techniques such as XFEM and CZM have been used to study repair damage with the development of numerical research (Talebi & Abedian, 2016; Talebi, Abedian, & Firooz, 2016; Bellali et al., 2021). In this context Bellali et al. (2020) have analysed crack propagation and adhesive debonding. They found that the damage varies depending on the interface strength and the effect of the notch in the repaired panel. Djebbar et al. (2021) have shown that the modelling techniques used correlate well with the experimental results, allowing the performance of the repair to be optimized.

The aim of this study is to evaluate the effectiveness of bonded composite patch repairs on notched marine steel structures subjected to tensile loading, by examining the mechanical behaviour of steel repaired with different types of structural adhesives. The tests are designed to ensure maximum reduction of stress concentrations around the notches and to extend the life of the repaired structure by determining how these adhesives affect the durability and strength of the repair under tensile loading.

Model Preview

Geometric Model and Mechanical Properties

The study is focused on a DH-36 marine-grade steel plate with a thickness of 2 mm, a length Hp=140 and a width Wp=40. The plate has a central circular hole with a radius of R=10 mm. This geometry was chosen to evaluate the performance of the repair technique using a composite patch. For the repair, a 1.5 mm thick composite patch was used. This part was bonded to the surface of the plate with a 0.2 mm thick layer of structural adhesive. The configuration and dimensions of the repaired area are detailed in Figure 1. Both the patch and the adhesive layer have the same dimensions.

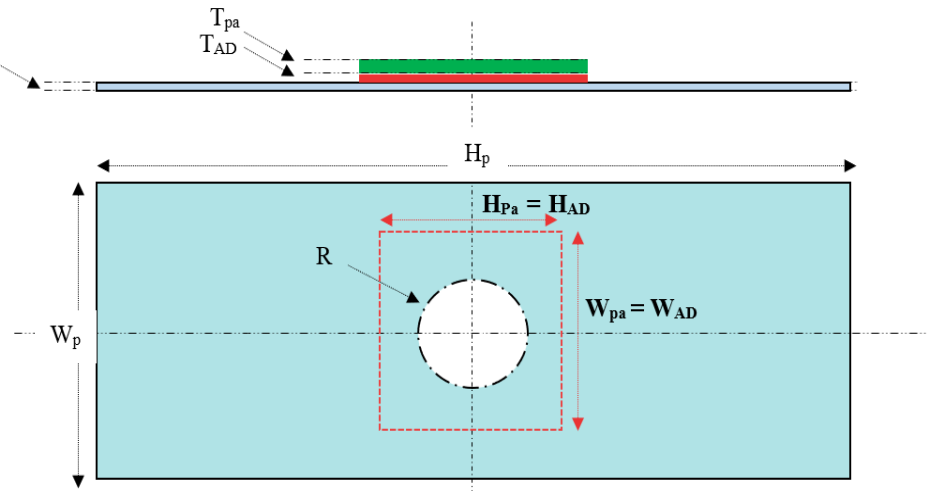

Figure 1. Geometric model presentation.

This study evaluates DH-36 steel, widely used in the marine industry for its excellent mechanical properties, particularly high strength and toughness. Its mechanical properties are detailed in Table 1. For the construction

of marine structures exposed to harsh conditions such as high stress environments and dynamic loads, DH-36 steel is often preferred.

Table 1. Mechanical properties of Dh-36 steel (Gao & Zhang, 2010).

Dh-36 Steel	
Young's modulus E (MPa)	200000
Poisson's ratio, ν	0.3
Shear modulus G (MPa)	76000
Elongation at fracture	0.126
Yield strength	636
Tensile strength	352

Three types of adhesives were examined: Adekit A-140, Araldite AV-138, and Sikaforce 7752. These adhesives were selected for their distinct mechanical properties, enabling the assessment of their respective performance in reinforcement applications. The mechanical characteristics of each adhesive are summarized in Table 2.

Table 2. Mechanical properties of adhesives (Djebbar et al., 2022; Santos & Campilho, 2017).

Property	Adekit-A140	Araldite-AV138	Sikaforce-7752
Young's modulus E (GPa)	2.6	4.89	0.49
Poisson's ratio, ν	0.3	0.35	0.30
Shear modulus G (GPa)	1	1.56	0.19
Tensile strength, σ_f	35.9	39.45	11.48
Shear strength, τ_f	30.9	30.2	10.17
Thoughness in tension, G_{IC}	0.5	0.20	2.36
Thoughness in shear, G_{IIC}	2.41	0.38	5.41

A carbon fiber reinforced polymer (CFRP) composite patch is used as the reinforcing material. This patch consists of 8 layers of 0.1875mm thickness, the stacking sequence follows an alternating orientation: $[0°/90°]_4$ to ensure optimal distribution of longitudinal and transverse stress. Table 3 shows the mechanical properties of the CFRP patch. Figure2 shows the tensile curves of the various materials used in this study.

Table 3. Mechanical properties of CFRP patch (Djebbar et al., 2022).

Carbon/Epoxy patch	
E_1 (MPa)	216525
E2 (MPa)	9860.94
E3 (MPa)	9860.94
Nu_{12}	0.37
Nu_{13}	0.37
Nu_{23}	0.37
G_{12} (MPa)	5340
G_{13} (MPa)	5340
G_{23}(MPa)	4338

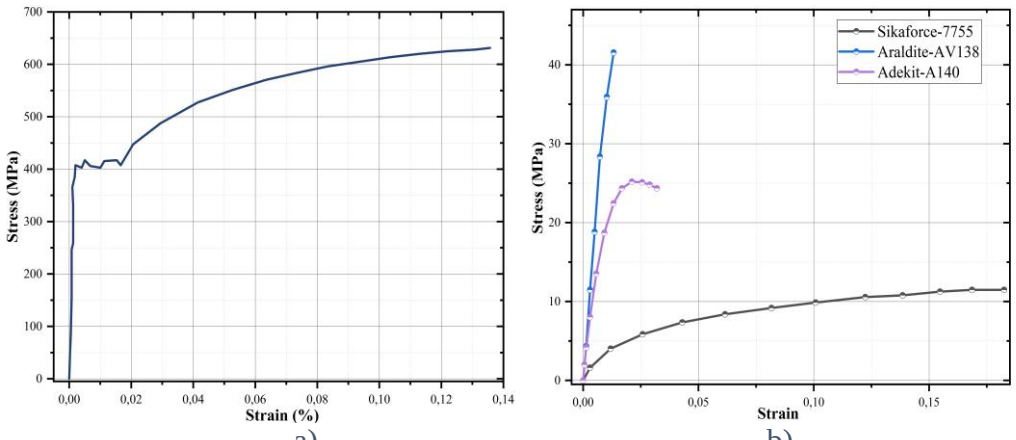

a) b)

Figure 2. a) Tensile test curve of Dh-36 steels, b) Stress strain curves of different adhesives used in this study (Gao & Zhang, 2010; Santos & Campilho, 2017).

Boundaray Conditions

In order to evaluate the performance of the repair process, the repaired DH-36 steel plate was subjected to a uniaxial tensile test (Figure 3). The test configuration is described below:

- *Zone A*: Fully constrained in all three displacement directions U_1, U_2 and U_3 ($U_1=U_2=U_3=0$ fixed along the x, y, and z axes), with free rotation around these axes ($UR_1=UR_2=UR_3 \neq 0$).
- *Zone B*: (opposite side): Partially constrained, with displacements blocked along U_2 and U_3 ($U_2=U_3=0$), but with free rotation around all three axes. Along the longitudinal axis U_1, a displacement of 15 mm (U_1 =15mm) has been applied.

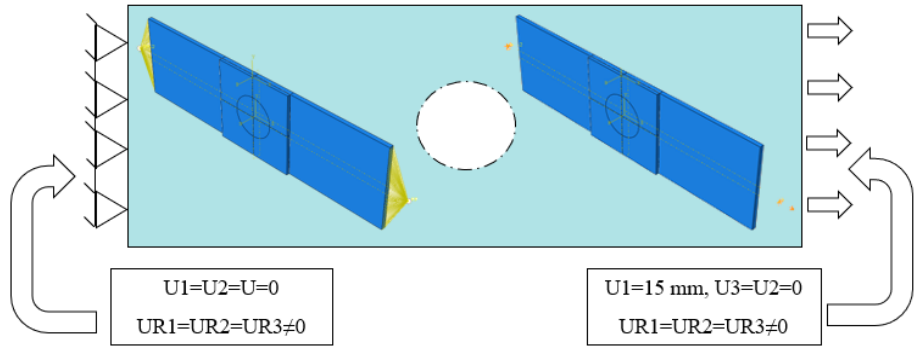

Figure 3. Boundary condition of present tensile test

Numerical Model

Finite element modelling was used to model and mesh the three components of this study (plate, adhesive and patch) in a three-dimensional model (**Hata! Başvuru kaynağı bulunamadı.**). where for the plate and patch, an element size of 1 mm was used, with C3D8R type elements. For the adhesive, COH3D8 cohesive elements of the same size were used. This was done to accurately capture the interactions between the plate, adhesive and the patch. The total number of elements used in the numerical model is shown in Table 3

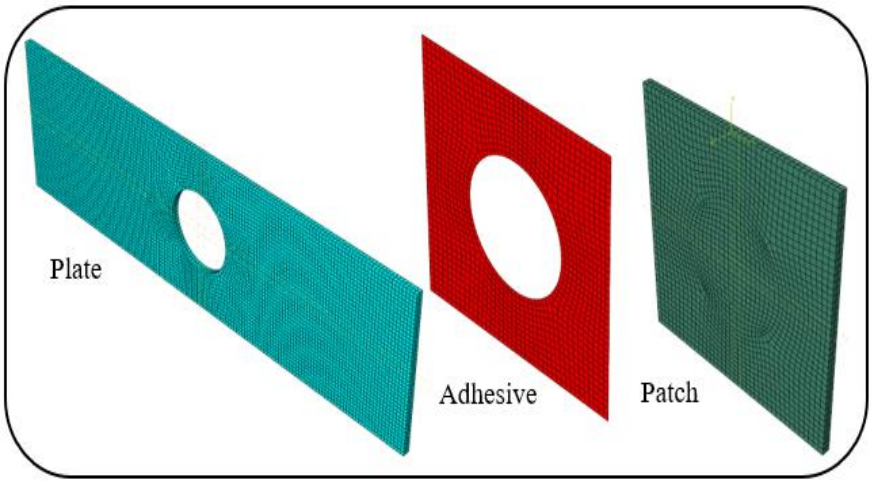

Figure 4. Numerical mesh presentation

Table 3. Numbers of mesh size elements.

Parts	Numbers of elements	Elements types
Plate	10696	C3D8R
Adhesive	1348	COH3D8
Patch	3488	C3D8R
Total number of elements	15532	

Method

In this present work, two numerical modelling approaches have been applied due to their importance in assessing damage in the plate, the adhesive and the patch. The extended finite element method (XFEM) is being applied to modelling the crack propagation in the plate, while the Cohesive Zone Method (CZM) provides the opportunity to simulate the cohesive behaviour of the adhesive used, and also simulate the deboning during the test. These two approaches together offer a thorough understanding of the damage mechanism.

Extended Finite Elements Modelling (XFEM)

This method makes the simulation more efficient as it is based on the concept of partitioning the finite element unit by using enrichment functions, which adds specific degrees of freedom to the nodes crossed by the crack or close to the crack tips, eliminating the need for re-meshing at each time unit and ensuring the fluidity of the crack propagation simulation. The XFEM method's mathematical formulation is given by the following equation:

$$U_{XFEM}(X) = \sum_{i\epsilon J} N_i(X)\, U_i + \sum_{i\epsilon J} N_i(X)\, H(X) a_i + \sum_{i\epsilon K} N_i(X)\, F(X) b_i \quad (1)$$

With, I represent the set of all mesh nodes, J and K are the nodes enriched by the Heaviside function $H(X)$ and the crack tip function $F(X)$.The nodal form functions $N_i(X)$ are employed to interpolate the standard displacements U_i and the enriched displacements a_i et b_i . The terms associated with $H(X)$ modelling the discontinuity in the elements traversed by the crack, while the terms linked to $F(X)$ capture the stress singularities near the crack tip.

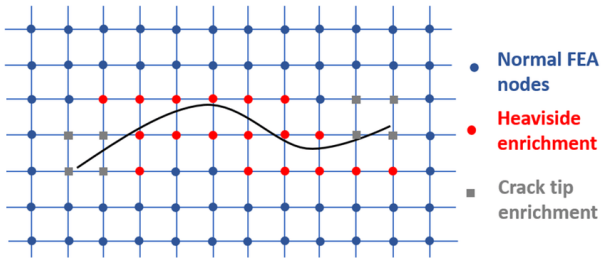

Figure 5. Enriched nodes in the XFEM (Gairola & Jayaganthan, 2021).

The discontinuity through the crack is modelled by the Heaviside function, given by the following equation (22*)*

$$H(X) = \begin{cases} 1 & if \quad x > 0 \\ -1 & if \quad x < 0 \end{cases} \quad (2)$$

This function makes it possible to model the discontinuity in the displacement field of the elements transverse to the crack without having to divide these elements. On the other hand, the improvement in accuracy at the crack point provided by the crack tip functions where stresses are highest. These functions, expressed in polar coordinates (r, θ), capture the singularities of the stress field near the crack tip and are defined by:

$$F_\alpha(r,\theta) = \left[\sqrt{r}\sin\left(\frac{\theta}{2}\right), \sqrt{r}\cos\left(\frac{\theta}{2}\right), \sqrt{r}\sin(\theta)\sin\left(\frac{\theta}{2}\right), \sqrt{r}\sin(\theta)\cos\left(\frac{\theta}{2}\right)\right] \quad (3)$$

Giving r as the distance to the crack and θ as the angle in polar coordinates. The initiation of crack propagation is controlled by the maximum principal stress criterion (MAXPS), which evaluates the maximum principal stress (MAXPS) in the enriched elements in ratio to the critical stress according to the relationship (4)

$$\left\{\frac{\sigma_{max}}{\sigma_{max_0}}\right\} = 1 \quad (4)$$

Once the stress exceeds the critical limit, crack initiation begins.

Cohesive Zone Modelling (CZM)

In present work, the numerical model is based on the evolution of damage between the adhesive surfaces of the plate and the patch by the linear traction-separation law, which gives the ability to track which deduce by the relationship (5)

$$T(\delta) = K.\delta \tag{5}$$

Where K is the stiffness matrix and δ represents the relative displacement of the contact surfaces, T is the nominal traction stress vector. In this way, we can also write

$$T = \begin{Bmatrix} T_n \\ T_s \\ T_t \end{Bmatrix} = \begin{bmatrix} K_{nn} & K_{ns} & K_{nt} \\ K_{ns} & K_{ss} & K_{st} \\ K_{nt} & K_{st} & K_{tt} \end{bmatrix} . \begin{Bmatrix} \varepsilon_n \\ \varepsilon_s \\ \varepsilon_t \end{Bmatrix} \tag{6}$$

The parameters K_{nn} and K_{ss} and K_{tt} are respectively the stress normal stiffness, the shear stiffness in the tangential direction 1, and the shear stiffness in the tangential direction 2 (Figure 6), and ε_n, ε_s and ε_t are the separations corresponding to the three directions.

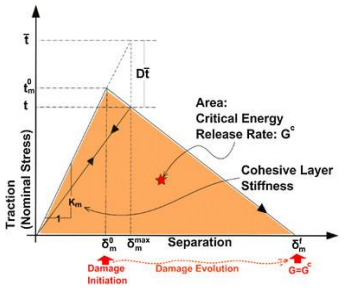

Figure 6. Linear traction-separation law for CZM (Haddad & Sepehrnoori, 2016).

The quadratic nominal stress criterion (QUADS) is chosen for damage initiation in our model, since this criterion assumes that damage begins when a quadratic interaction function involving the nominal strain ratios is represented by the following formula

$$\left(\frac{T_n}{T_n^0}\right)^2 + \left(\frac{T_s}{T_s^0}\right)^2 + \left(\frac{T_t}{T_t^0}\right)^2 = 1 \tag{7}$$

T_n, Ts et T_t are the nominal stresses in normal (tension), shear 1 and shear 2 modes, and T_n^0 , T_s^0 et T_t^0 are the corresponding critical stresses. The damage evolution is modelled by the energy dissipation according to the Benzeggagh-Kenane criterion which takes into account the separation in the mixed modes (tension and shear) according to the following relationship (8)

$$G_{IC} + (G_{IiC} + G_{IC}).\left(\frac{G_s}{G_T}\right)^n = G_c \tag{8}$$

where $G_s = G_{IiC} + G_{IC}$, $G_t = G_{IC} + G_s$ and η a characteristic material parameter, G_{IC} , G_{IIC} and G_{IIIC} represent the energy restitution rates for the modes I, II, et III

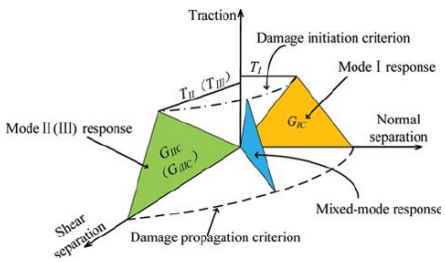

Figure 7. Mixed mode traction separation law (Hu et al., 2014).

Results and Discussion

Effect of Adhesively Bonded Patch

The results of the load-displacement curves for the repair using a patch are presented in Figure 8. The maximum recorded loads are 28 kN and 21 kN for the repaired and damaged plates, respectively. Consequently, there has been an improvement of 33% in strength compared to the notched plate. Moreover, a notable discrepancy in the post-peak load levels across the various tests is evident, wherein the repaired plate exhibits a gradual decrease, in contrast to the damaged one, which displays a precipitous reduction. This suggests that the repair enhances the ductility of the structure. The findings illustrate that the patch, bonded with structural adhesive in the damaged marine structure, plays a pivotal role in the load redistribution process.

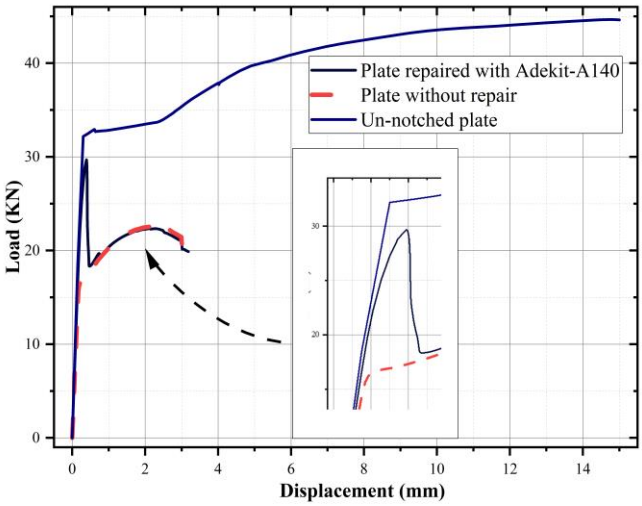

Figure 8. Load-displacement of repaired, notched and un-notched plate.

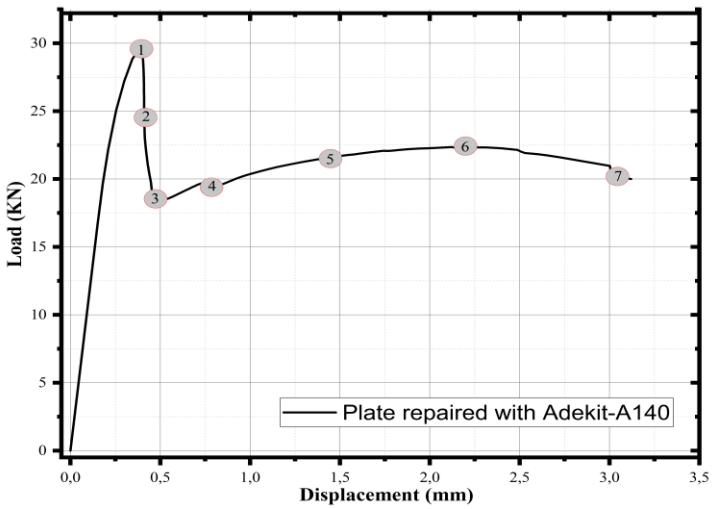

Figure 9. Load-displacement curve with points corresponding to stress analysis stages.

Stress Distribution Evaluation

It is essential to monitor the stress distribution in order to analyse the performance of the repair. Figure 9 shows the load-displacement curve, marked by numbered points corresponding to the detailed analysis frames of the von Mises σ_{mises} stresses in the plate and adhesive, as well as the S_{11} stresses in the loading direction presented in **Hata! Başvuru kaynağı bulunamadı.**. When the load reaches its maximum value of 28 kN, a significant stress concentration is recorded in the plate. The adhesive plays a key role in load transfer, with high stresses concentrated at its edges. The patch also shows high levels of stress, absorbing some of the load to lighten the plate and support the overall structure.

Table 4. Stress distribution in the plate, adhesive and patch.

Frame	Plate	Adhesive	Patch
(1)	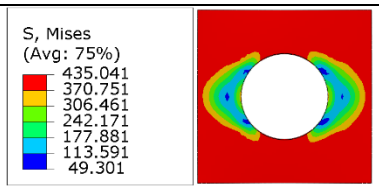	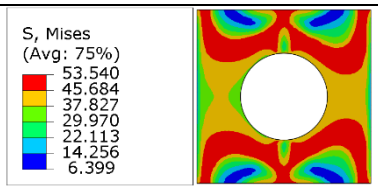	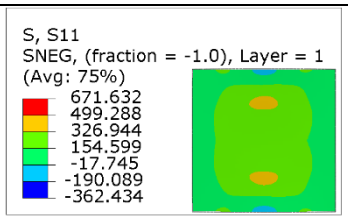
(2)	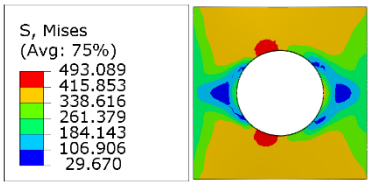	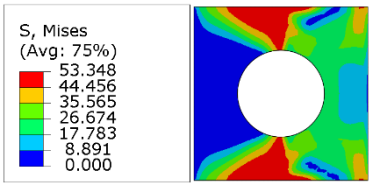	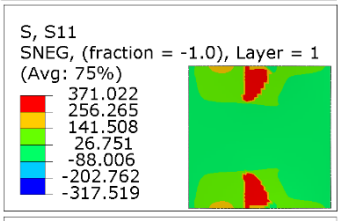
(3)	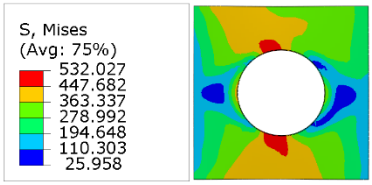	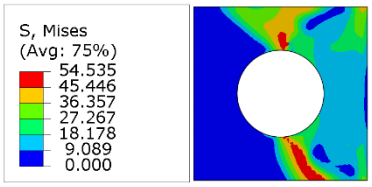	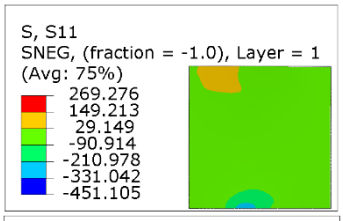
(4)	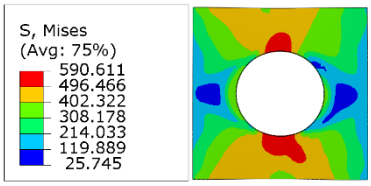	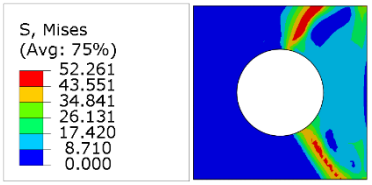	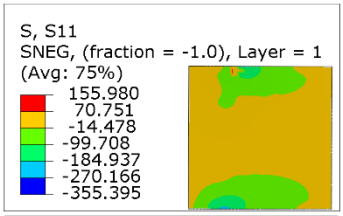
(5)	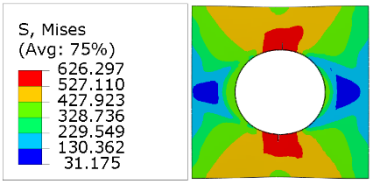	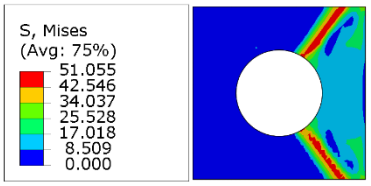	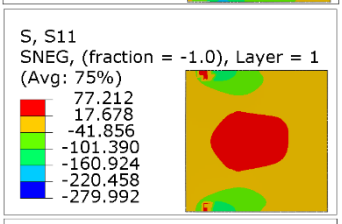
(6)	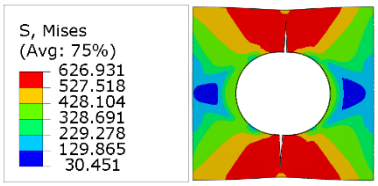	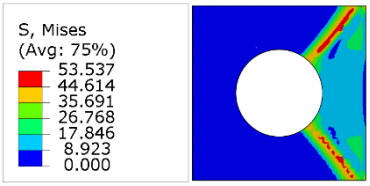	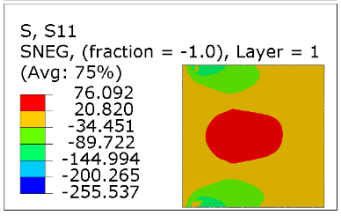
(7)	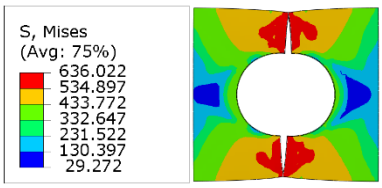	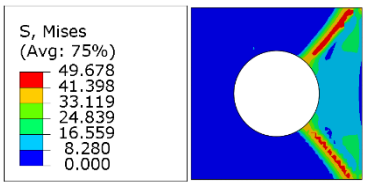	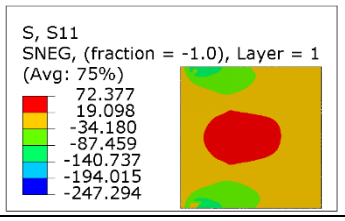

Subsequently, stresses increase rapidly in the plate, while the adhesive maintains a stable stress level around 52 MPa on average. However, signs of debonding begin to appear and progress quickly due to the high loads transferred from the plate. This debonding causes a gradual decrease in stress within the patch. As the process continues, a crack initiates in the plate and propagates rapidly as the adhesive debonding extends, leading to failure at a maximum stress level of 636 MPa in the plate. At the point of rupture, the patch reaches a stress level of 72 MPa, indicating a reduced contribution to structural support due to the diminished load absorption from the adhesive debonding.

Effect of Adhesives Natur

The effect of the strength of different adhesives was analysed by means of stress-strain curves, as illustrated in Figure 10. The results demonstrate that the Adekit-A140 repair exhibits the most favourable performance and strength with steel in terms of overall efficacy when compared to Araldite AV-138 and Sikaforce 7752. Moreover, the A140 initially exhibits rigid behaviour, followed by a decrease in charge before reaching a stable peak load of approximately 24 kN, ultimately leading to the failure of the plate. The data suggests that energy is transferred and that the material undergoes favourable ductile behaviour once the peak load is reached.

Moreover, the results for Araldite AV-138 also illustrate a noteworthy performance, with a maximum load of 25 kN. Nevertheless, a rapid decrease in charge is observed after the peak, indicating that the adhesive in question performs well in the initial loading phase but has more limited bond strength at the interface. In contrast, the Sikaforce 7752 adhesive manifests reduced strength in comparison to the other adhesives, reaching a maximum of 22 kN. Additionally, upon reaching the maximum load, the Sikaforce 7752 exhibits a more pronounced loss of load, suggesting a more brittle behaviour. Such observations could indicate that this adhesive has a reduced capacity to retain residual stresses after damage initiation at the patch-plate interface.

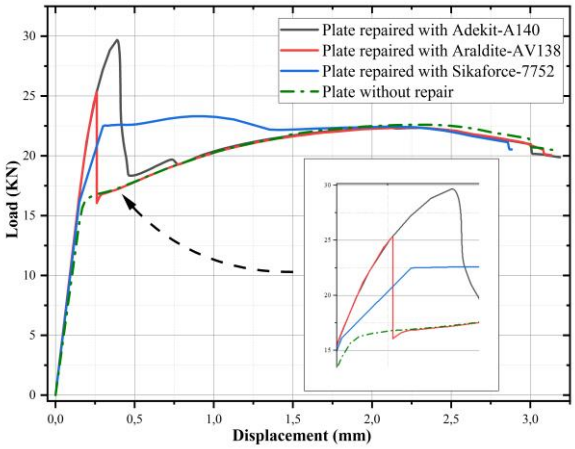

Figure 10. Load-displacement curve of different adhesives used.

Debonding Progression Views during Test

Table 5. Debonding progress views

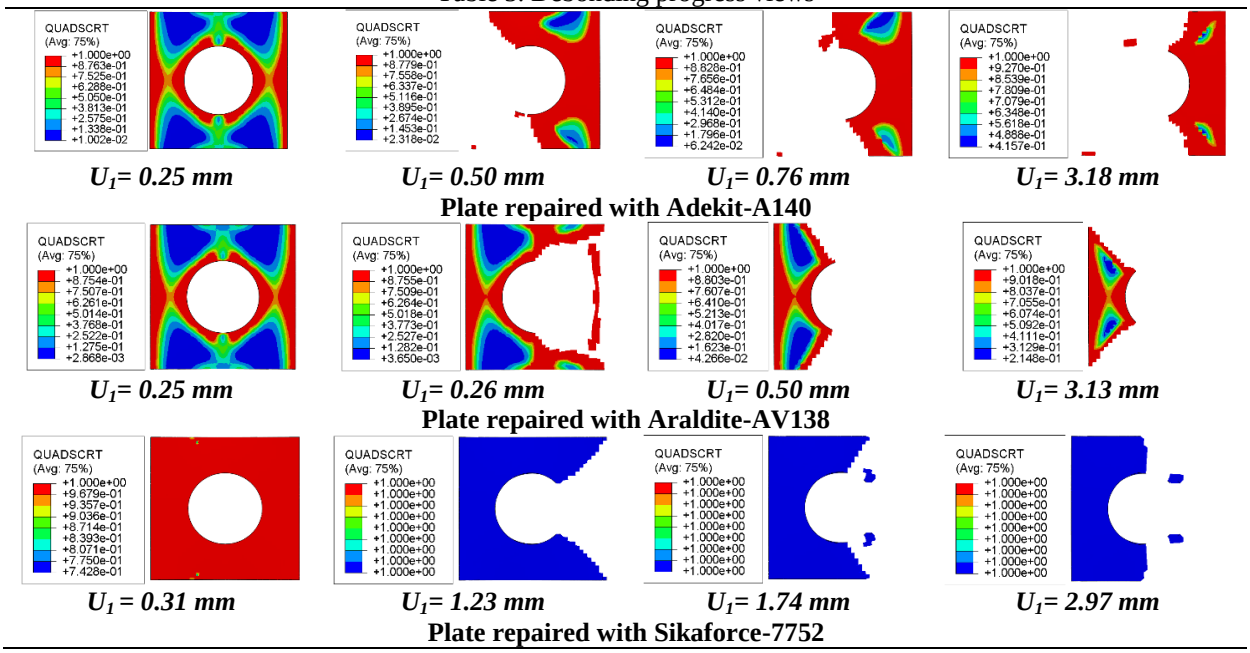

The monitoring of the delamination process in the repaired plate are presented in Table 5.. The analysis of delamination for the three adhesives (Adekit-A140, Araldite-AV138, and Sikaforce-7752) reveals a comparable damage progression, whereby delamination initiates and propagates at the edges of the patch as the longitudinal displacement U1 increases towards the notch.

For instance, for small displacements (U1 around =0.2 to 0.31mm), all adhesives demonstrate delamination zones that are limited to the opening. However, Sikaforce-7752 exhibits a slightly faster propagation rate. In contrast, at moderate displacements (U1 around 0.5 to 1.7 mm), all three adhesives display a notable progression in delamination. Moreover, at high displacements (U1=3mm), nearly the entire patch is delaminated, with extensive damage observed for all three adhesives. Although Sikaforce-7752 appears to delaminate more uniformly, the damage is nevertheless significant. Furthermore, the delamination progression observed in Adekit-A140 and Araldite-AV138 is relatively gradual, whereas Sikaforce-7752 demonstrates a more rapid initiation and propagation of damage.

Conclusion

This study presents a numerical analysis, using advanced finite element modelling techniques including the Extended Finite Element Method (XFEM) and Cohesive Zone Model (CZM) approaches, of the repair performance of damaged marine steel structures using bonded composite patch repair techniques.

- The results show that the type of adhesive plays a critical role in the repair performance of steel structures, directly influencing the evolution of the mechanical behaviour according to the specific properties of each adhesive.
- Adekit A-140 proved to be much more durable and stronger than those tested and provided better load retention.
- The debonding in each of the adhesives revealed the specific deboning phenomena of each type of adhesive, highlighting the importance of selecting a suitable adhesive to optimize the durability and effectiveness of the repair.

Scientific Ethics Declaration

The authors declare that the scientific ethical and legal responsibility of this article published in EPSTEM Journal belongs to the authors.

Acknowledgements or Notes

* This article was presented as a poster presentation at the International Conference on Technology, Engineering and Science (www.icontes.net) held in Antalya/Turkey on November 14-17, 2024.

References

Abbas, M., & Shafiee, M. (2020). An overview of maintenance management strategies for corroded steel structures in extreme marine environments. *Marine Structures, 71*, 102718.

Bellali, M. A., Mokhtari, M., Benzaama, H., Fekirini, H., Serier, B., & Madani, K. (2020). Using CZM and XFEM to predict the damage to aluminum notched plates reinforced with a composite patch. *Journal of Mechanics of Materials and Structures, 15*(2), 185-201.

Bellali, M. A., Serier, B., Mokhtari, M., Campilho, R. D. S. G., Lebon, F., & Fekirini, H. (2021). XFEM and CZM modeling to predict the repair damage by composite patch of aircraft structures. Debonding parameters. *Composite Structures, 266*, 113805.

Benyahia, F., Aminallah, L., Albedah, A., Bachir Bouiadjra, B., & Achour, T. (2015). Experimental and numerical analysis of bonded composite patch repair in aluminum alloy 7075 T6. *Materials & Design, 73*, 67-73.

Berrahou, M., & Amari, K. (2022). Experimental and numerical study on the efficiency of the repair of composite structures cracked and V-notched by different types and shapes of composite material patch. *Strojnícky Časopis - Journal of Mechanical Engineering, 72*(1), 1-14.

Breitzman, T. D., Iarve, E. V., Cook, B. M., Schoeppner, G. A., & Lipton, R. P. (2009). Optimization of a composite scarf repair patch under tensile loading. *Composites Part A: Applied Science and Manufacturing, 40*(12), 1921-1930.

Colak, Z., Ayan, Y., & Kahraman, N. (2020). Weld morphology and mechanical performance of marine structural steel welded underwater in a real marine environment. *The International Journal of Advanced Manufacturing Technology, 109*(1), 491-501.

Djebbar, S. C., Madani, K., El Ajrami, M., Houari, A., Kaddouri, N., Mokhtari, M., Feaugas, X., & Campilho, R. D. S. G. (2022). Substrate geometry effect on the strength of repaired plates: Combined XFEM and CZM approach. *International Journal of Adhesion and Adhesives, 119*, 103252.

Fekih, S. M., Albedah, A., Benyahia, F., Belhouari, M., Bachir Bouiadjra, B., & Miloudi, A. (2012). Optimisation of the sizes of bonded composite repair in aircraft structures. *Materials & Design, 41*, 171-176.

Feng, L., He, J., Hu, L., Shi, H., Yu, C., Wang, S., & Yang, S. (2020). A parametric study on effects of pitting corrosion on steel plate's ultimate strength. *Applied Ocean Research, 95*, 102026.

Gairola, S., & Jayaganthan, R. (2021). XFEM simulation of tensile and fracture behavior of ultrafine-grained Al 6061 alloy. *Metals, 11*(11), 1761.

Gao, X., & Zhang, G. (2010). A study on the effect of the stress state on ductile fracture. *International Journal of Damage Mechanics, 19(1),* 75-94.

Grabovac, I., & Whittaker, D. (2009). Application of bonded composites in the repair of ships structures – A 15-year service experience. *Composites Part A: Applied Science and Manufacturing, 40*(9), 1381-1398.

Haddad, M., & Sepehrnoori, K. (2016). XFEM-based CZM for the simulation of 3D multiple-cluster hydraulic fracturing in quasi-brittle shale formations. *Rock Mechanics and Rock Engineering, 49*(12), 4731-4748.

Hu, P., Shi, Z. W., Wang, X. X., Li, W. D., Zhou, S. G., & Han, X. (2014). Strength degradation of adhesively bonded single-lap joints in a cyclic-temperature environment using a cohesive zone model. *Journal of Adhesion, 91*(8), 587-603.

Iváñez, I., & Braun, M. (2018). Numerical analysis of surface cracks repaired with single and double patches of composites. *Journal of Composite Materials, 52*(8), 1113-1120.

Kaddouri, N., Madani, K., Rezgani, L., Mokhtari, M., & Feaugas, X. (2020). Analysis of the effect of modifying the thickness of a damaged and repaired plate by composite patch on the j-integral; effect of bonding defects. *Journal of the Brazilian Society of Mechanical Sciences and Engineering, 42*(8), 426.

Karatzas, V. A. (2016). *Assessment and design of composite patch repairing in marine applications*. file:///C:/Users/pc/Downloads/PhD_Vasileios_Karatzas.pdf.

Karatzas, V. A., Kotsidis, E. A., & Tsouvalis, N. G. (2015). Experimental fatigue study of composite patch repaired steel plates with cracks. *Applied Composite Materials, 22*(5), 507-523.

Li, C., Zhao, Q., Yuan, J., Hou, Y., & Tie, Y. (2019). Simulation and experiment on the effect of patch shape on adhesive repair of composite structures. *Journal of Composite Materials, 53*(28-30), 4125-4135.

Liu, Z., Li, Z., Huang, C., & Jiang, X. (2022). An investigation on the fatigue performance of cracked steel plates reinforced with FRP and stop hole. *Mechanics of Advanced Materials and Structures, 29*(25), 3646-3657.

Madani, K., Touzain, S., Feaugas, X., Cohendouz, S., & Ratwani, M. (2010). Experimental and numerical study of repair techniques for panels with geometrical discontinuities. *Computational Materials Science, 48*(1), 83-93.

Marioli-Riga, Z., & Gdoutos, E. E. (2004). Composite patch repair methodology for damaged aircrafts structural components. In *2004 SEM Annual Conference*, 7-10.

Mishra, K., Lal, A., & Sutaria, B. M. (2023). Experimental investigation of repair of plate with edge and center crack by surface bounded composite patch. *International Journal of Steel Structures, 23*(2), 534-547.

Mohammadi, S., Yousefi, M., & Khazaei, M. (2021). A review on composite patch repairs and the most important parameters affecting its efficiency and durability. *Journal of Reinforced Plastics and Composites, 40*(1-2), 3-15.

Riveros, G., Hassan, E. M., Hudak, L., & Mahmoud, H. (2022). Basalt fibers for underwater fatigue repair of steel panels. *Journal of Structural Engineering, 148*(11), 04022184.

Sadek, K., Aour, B., Bachir Bouiadjra, B. A., Bouanani, M. F., & Khelil, F. (2018). Analysis of crack propagation by bonded composite for different patch shapes repairs in marine structures. A numerical analysis. *International Journal of Engineering Research in Africa, 35*, 175-184.

Santos, M. A. S., & Campilho, R. D. S. G. (2017). Mixed-mode fracture analysis of composite bonded joints considering adhesives of different ductility. *International Journal of Fracture, 207*(1), 55-71.

Shivaie- Kojouri, A., Safarabadi, M., & Parvas, D. (2023). A numerical comparison between aged and non-aged composite patches on repaired aluminum 7075-T6 plate. *Materials Chemistry and Mechanics, 1*(1),74-87.

Silva, D. L., Echer, L., Rojo Tanzi, B. N., Marczak, R. J., & Iturrioz, I. (2023). Experimental investigation of the structural performance of fiber-reinforced patches in the repair of locally damaged steel pipes. *Journal of the Brazilian Society of Mechanical Sciences and Engineering, 45*(8), 435.

Soutis, C., & Hu, F. Z. (1997). Design and performance of bonded patch repairs of composite structures. *Proceedings of the Institution of Mechanical Engineers, Part G: Journal of Aerospace Engineering, 211*(4), 263-271.

Talebi, B., & Abedian, A. (2016). Numerical modeling of adhesively bonded composite patch repair of cracked aluminum panels with concept of CZM and XFEM. *Proceedings of the Institution of Mechanical Engineers, Part G: Journal of Aerospace Engineering*, *230*(8), 1448-1466.

Talebi, B., Abedian, A., & Firooz, S. (2016). Optimization of composite patch repair for inclined crack on aluminum plate using genetic algorithm. *Archive*, *231*(20).

Yu, Q. Q., Zhao, X. L., Al-Mahaidi, R., Xiao, Z. G., Chen, T., & Gu, X. L. (2014). Tests on cracked steel plates with different damage levels strengthened by CFRP laminates. *International Journal of Structural Stability and Dynamics*, *14*(06), 1450018.

Zhang, Y., Zhang, K., Zhao, H., Xin, J., & Duan, M. (2018). Stress analysis of adhesive in a cracked steel plate repaired with CFRP. *Journal of Constructional Steel Research*, *145*, 210-217.

Author Information

Harmel Mohammed Walid
Djilali Liabes University of Sidi-Bel-Abbes
BP 89, Sidi Bel Abbes 22000, Algeria
Contact e-mail: harmelwalid03*@gmail.com*

Zouggar Kamel
Djilali Liabes University of Sidi-Bel-Abbes
BP 89, Sidi Bel Abbes 22000, Algeria

Baghdadi Mohammed
Djilali Liabes University of Sidi-Bel-Abbes
BP 89, Sidi Bel Abbes 22000, Algeria

Mhamdia Rachid
Djilali Liabes University of Sidi-Bel-Abbes
BP 89, Sidi Bel Abbes 22000, Algeria

To cite this article:

Walid, H.,M., Kamel, Z., Mohammed, B. & Rachid, M. (2024). Numerical damage prediction of marine structures reinforced by composite patch with XFEM and CZM methods. *The Eurasia Proceedings of Science, Technology, Engineering & Mathematics (EPSTEM), 32*, 173-184.